NATIONAL ADVISORY COMMITTEE FOR AERONAUTICS

TECHNICAL NOTE

No. 1373

CHARTS FOR THE DETERMINATION OF SUPERSONIC AIR FLOW AGAINST INCLINED PLANES AND AXIALLY SYMMETRIC CONES

By W. E. Moeckel and J. F. Connors

Flight Propulsion Research Laboratory
Cleveland, Ohio

Washington
July 1947

NATIONAL ADVISORY COMMITTEE FOR AERONAUTICS

TECHNICAL NOTE No. 1373

CHARTS FOR THE DETERMINATION OF SUPERSONIC AIR FLOW AGAINST INCLINED PLANES AND AXIALLY SYMMETRIC CONES

By W. E. Moeckel and J. F. Connors

SUMMARY

A set of charts is presented for the convenient determination of flow conditions behind a shock wave and at the surface of inclined planes and axially symmetric cones located in a uniform frictionless supersonic air stream. Shock angle, static-pressure coefficient, static-pressure ratio, total-pressure ratio, Mach number ratio, and velocity ratio for two-dimensional and conical flow fields are plotted for a range of free-stream Mach numbers from 1.05 to infinity. The charts for two-dimensional flow were calculated from theoretical relations for oblique shocks in frictionless air streams. The charts for flow against cones were obtained from solutions previously reported. A chart of the Prandtl-Meyer relations for two-dimensional isentropic flow around corners is also presented.

INTRODUCTION

The deflection of a uniform supersonic air stream produced by any obstacle in the stream results in the formation of a shock wave. As the air flows through this shock wave, it is compressed (raised to a higher static pressure) and its velocity is reduced. Because the entropy of the air increases in passing through a shock, the total pressure of the air stream is also reduced. If the shock is not normal to the free-stream flow direction, the flow direction is changed in passing through the shock. The theory of compression shocks indicates that, if friction is neglected, the conditions immediately behind the shock are completely determined by the conditions of the free stream and the angle between the shock wave and free-stream flow directions. In order to predict the conditions at the surface of an obstacle in the stream or in the field between the shock and the surface, it is therefore necessary to know the relation between the geometry of the obstacle and the angle of the resulting shock. This relation has been determined for only a few simple, but very important, geometric elements, among which are the inclined

plane surface and the axially symmetric cone. The charts presented are intended to provide, in convenient and complete form, the theoretical relations required to determine the supersonic flow against these two types of obstacle and the conditions immediately behind any shock when its direction is known. The equations used to compute the charts for flow conditions behind a shock and on the surface of an inclined plane were derived from those given in reference 1. The charts of the conditions on cone surfaces were constructed from data presented in references 2 to 4. A chart giving the Prandtl-Meyer relations for supersonic flow around corners (discussed in reference 5) is also presented.

SYMBOLS

The following symbols are used in this report:

a	local sound velocity
a_{cr}	critical velocity, $\left(\frac{2\gamma}{\gamma-1} gRT\right)^{1/2}$
g	gravitational constant
L	velocity component parallel to shock
M	Mach number
M_{cr}	ratio of free-stream velocity to critical velocity, (q_0/a_{cr})
P	total pressure
p	static pressure
q	velocity
R	gas constant
T	total temperature
t	static temperature
u,v	velocity components parallel and perpendicular, respectively, to the free-stream direction
β	Mach angle

φ angle between shock and flow direction ahead of shock

γ ratio of specific heats

λ angle between flow ahead of and behind shock

θ_c cone half-angle

θ_w angle between inclined plane and free-stream direction

ρ density

ψ angle through which flow is expanded (Prandtl-Meyer theory)

Subscripts:

0 conditions in stream before shock

1 conditions behind shock (or before Prandtl-Meyer expansion)

2 conditions after Prandtl-Meyer expansion

c conditions on cone surface

w conditions on surface of inclined plane

cr critical values

max maximum values

DESCRIPTION OF TWO-DIMENSIONAL AND CONICAL FLOW

A sketch of a wedge with one surface parallel to the free-stream direction and the other surface inclined at an angle θ_w is presented in figure 1. The flow of a frictionless supersonic air stream against such a wedge may be described as follows: As the air stream passes through the shock attached to the leading edge of the wedge, it is deflected upward through an angle λ. If θ_w is less than a certain maximum value, λ_{max} dependent on the free-stream Mach number M_0, the shock is attached to the leading edge (fig. 1). The flow direction is then constant in the entire field between shock and surface; the surface angle is equal to the angle of deflection through the oblique shock ($\lambda = \theta_w$). The compression of the flow, which must result from such a deflection, takes place abruptly through

the oblique shock wave emanating from the leading edge. If the wedge is assumed to extend an infinite distance downstream, the oblique shock is straight and of constant intensity to infinity, which means that (a) the flow is deflected an equal amount wherever it passes through the shock and (b) conditions behind (downstream of) the shock are everywhere equal. The intensity of the shock for a given value of M_0 is a function of the shock angle φ, which is in turn dependent only on λ. For $\theta_w = \lambda = 0$, there is no flow deflection or compression and the shock wave becomes a Mach wave. The shock angle φ is then equal to the Mach angle $\beta = \sin^{-1}1/M_0$. As θ_w is increased, the shock angle and, consequently, the shock intensity increase. When θ_w reaches a certain critical value λ_{cr}, which depends on M_0, the flow behind the shock becomes sonic $(M_1 = 1.0)$. For values of θ_w greater than λ_{cr} the flow behind the shock is everywhere subsonic $(M_1 < 1.0)$.

When θ_w reaches a certain maximum value λ_{max} (slightly greater than λ_{cr}) the shock wave becomes curved and stands upstream of the leading edge. The flow behind the shock is no longer uniform; the deflection of the flow in passing through the shock varies from point to point, depending on the angle of the shock at that point. The angle of deflection of the flow λ is no longer to be identified with the surface inclination θ_w and the conditions on the surface are no longer the same as those immediately behind the shock.

As θ_w is further increased beyond λ_{max}, φ and p_1 continue to increase, but λ decreases. When θ_w reaches 90°, the shock wave is normal to the free-stream direction over the entire area ahead of the surface and the flow deflection through the shock is zero.

If the shock is attached to the leading edge of the surface, the flow past the lower surface of the wedge shown in figure 1 remains unaffected because it is parallel to the free-stream direction. When the shock becomes detached, however, the flow from the upper region, which is now subsonic and at a higher pressure than the free stream, will expand around the leading edge into the lower region. This expansion will result in a compressive deflection of the free stream in that region and a consequent extension of the shock wave into the lower region. When θ_w exceeds λ_{max}, a complete bow wave will therefore appear, which is normal to the free stream just ahead of the leading edge. The lower half of the wave, however, will degenerate into a Mach wave at some distance from the wedge because the

flow behind the shock is expanding to free-stream conditions. On the other hand, if the wedge is of infinite extent as assumed, the upper half of the shock wave maintains a finite intensity.

A description of supersonic flow past a symmetrical cone with the axis parallel to the free-stream direction (fig. 2) is analogous in several respects with the description of flow over inclined surfaces given previously. The shock angle and the shock intensity again vary continuously with cone half-angle θ_c up to a maximum value $\theta_{c,max}$ beyond which the shock becomes detached from the cone tip and stands ahead of the cone as a bow wave. The important difference lies in the fact that, even with the shock attached, the conditions in the field between the shock and the cone are not constant. After the compression through the shock wave, there is a further compression of the flow between the shock and the cone surface. The streamlines behind the shock are therefore curved and the cone half-angle θ_c cannot be identified with the angle of flow deflection through the shock λ. The condition of the flow immediately behind the shock, however, is determined from the oblique-shock relations previously described if the shock angle φ is known. The relation between this shock angle and the cone angle and the conditions on the cone surface must be determined by integrating the differential equation for axially symmetric conical flow. This equation has been derived, in different forms, by Taylor and Maccoll (references 2 and 3) and by Busemann (reference 6). The authors of references 2 and 3 carried out the integration of their equation for Mach numbers up to 8 and for shock angles up to those obtained for $\theta_{c,max}$. The integration of Busemann's equation was carried out by Hantzche and Wendt (reference 4) for Mach numbers to infinity and for all shock angles. No attempt has been made in this paper to recalculate the results. The over-all agreement between the two independent calculations already made is deemed sufficient to assure their accuracy. The data for the charts on conical flow were merely replotted and cross-plotted in this report for the sake of completeness and greater accessibility. These charts apply only to cones at an angle of attack of 0. Theoretical discussions of conical flow at angles of attack may be found in references 7 and 8.

The preceding discussion is concerned only with deflections of the flow resulting in compression. Conditions resulting from an expansion of the flow around a portion of an obstacle inclined away from the flow direction, such as the trailing portion of a wing, can also be theoretically determined. If the flow is two dimensional, the Prandtl-Meyer theory for expansion around corners is used

(reference 5). A chart is included in this paper giving the Prandtl-Meyer relations up to a Mach number of 4. The use of this chart is subsequently described.

DESCRIPTION OF CHARTS

Total-pressure ratio across shocks. - Because the compression of the flow through a shock is not isentropic, the total pressure of the stream behind the shock is less than that of the free stream. The ratio of the total pressures behind and ahead of the shock P_1/P_0 depends only on the shock angle φ and on the Mach number before the shock M_0. (See appendix, equation (16).) This relation is plotted in figure 3 for values of M_0 from 1.2 to 15.0. Because the additional compression between the shock and the cone surface is assumed to be isentropic, this chart may be used to find the total pressure in a conical as well as a two-dimensional field. The intercepts of these curves at $\varphi = 90^\circ$ correspond to a normal shock, whereas the other limits of the curves at $P_1/P_0 = 1.0$ correspond to the Mach angles.

Change in flow direction, static pressure, and Mach number across oblique shocks. - The oblique-shock relations between angle of flow deflection λ and shock angle φ, static-pressure coefficient $\frac{(p_1/p_0) - 1}{\gamma M_0^2}$, static-pressure ratio p_1/p_0, and Mach number ratio M_1/M_0 are plotted in figures 4, 5, 6, and 7, respectively, for several free-stream Mach numbers M_0. The flow against inclined plane surfaces is directly determined from these charts.

In these figures, two shock solutions are given for each $\lambda < \lambda_{max}$. When a plane surface is inclined at an angle $\theta_w < \lambda_{max}$, the solution indicated by the solid lines is by far the more likely to occur in practice. There is experimental evidence, however, that the dotted-line solutions occur under special conditions (reference 9). Except for such special cases, the dotted upper portions of the curves are useful in practice for determining only the flow conditions immediately behind various portions of a detached shock wave if the angle of the wave is known at each point. If a detached shock is a complete bow wave, whose angle φ with the free-stream direction varies from 90° down to the Mach angle, then each point of the curves for a given value of M_0 is represented by a point on the bow wave occurring at that value of M_0. The form of such a bow wave has not yet been theoretically determined but must be determined by experiment.

The theoretical determination is complicated because for such shocks, a mixture of subsonic and supersonic flow exists in the field behind the shock and because the field is not uniformly isentropic.

As an example of the use of the charts in figures 3 to 7, consider a symmetrical wedge of half-angle $\theta_w = 10^\circ$ at an angle of attack of 0° in an air stream of Mach number $M_0 = 2.0$. In figure 4, the shock angle φ is 39.2°. The static-pressure coefficient from figure 5 is 0.128 and the static-pressure ratio p_1/p_0 is 1.7 (fig.6). The ratio of the Mach number in the field behind the shock M_1 to the free-stream Mach number M_0 from figure 7 is 0.82; therefore, M_1 is 1.64. From figure 3, the total-pressure ratio is found to be 0.983.

The values of λ in figure 7 for which M_1 reaches 1.0 are slightly less than λ_{max}; that is, the flow behind the shock is already slightly subsonic before shock detachment occurs. For $M_0 = 2.0$, for example, $M_1/M_0 = 0.5$ when $\lambda = 22.7^\circ$, whereas $\lambda_{max} = 22.95^\circ$.

Flow past axially symmetric cones. - Graphical solutions of the differential equation for the axially symmetric conical field have been determined for all shock angles and all free-stream Mach numbers in reference 4. The shock angle and the pressure coefficient are plotted in reference 4 against cone half-angle for various values of M_{cr}. These two charts are replotted in figures 8 and 9 for various values of M_0, which is a simple function of M_{cr}. (See appendix, equation (7).) The integrations carried out in references 2 and 3 were less comprehensive than those in reference 4 and covered only the solid-line solutions (figs. 8 and 9) for Mach numbers up to 8.0. Within this range, the two methods were compared at a number of points and were found to be in complete agreement within the error in reading the values from the respective charts. This error in readability was about $\pm 0.5^\circ$ for the shock angle and about ± 0.01 for the pressure coefficient. Figures 8 and 9, although plotted on a more readable scale, are therefore limited to the accuracy of the reference charts. The fairing of curves through the points, however, should average out some of the reading errors.

An examination of figure 8 shows that the shock angle φ increases with half-angle of the cone θ_c up to a maximum angle $\theta_{c,max}$, which is considerably greater than λ_{max} found for two-dimensional flow (fig. 4). Again there are two solutions for the shock angle at each $\theta_c < \theta_{c,max}$. In this case, however, no experimental evidence is known for the occurrence of the broken-line solutions. The flow conditions immediately behind a conical shock

are still determined from the two-dimensional oblique shock relations of figures 3 to 7 once the shock angle φ has been determined for a particular cone angle.

The pressure coefficient at the surface of the cone $\frac{(p_c/p_0) - 1}{\gamma M_0^2}$ is plotted against cone half-angle θ_c for all values of M_0 in figure 9.

The ratio of static pressure on the cone surface p_c to the free-stream static pressure p_0 is plotted for $M_0 = 1.05$ to 2.0 in figure 10(a), for $M_0 = 2.0$ to 6.0 in figure 10(b), and for $M_0 = 6.0$ to 15.0 in figure 10(c). The data were calculated from figure 9. At $\theta_c = 0$, the static pressure at the cone surface p_c is the same as the static pressure behind the shock p_1, both for the normal-shock solution and for the Mach angle solution. (Compare figs. 9 and 10 with figs. 5 and 6)

The ratio of the Mach number at the cone surface M_c to the free-stream Mach number M_0 is plotted against cone half-angle in figure 11(a) for $M_0 = 1.05$ to 2.0 and in figure 11(b) for $M_0 = 2.0$ to 15.0. These curves were calculated from the pressure ratios of figures 6 and 10, as explained in the appendix (equation (18)). The critical θ_c, for which the surface Mach number M_c is 1.0, does not closely correspond with the maximum angle for which the shock remains attached to the cone tip $\theta_{c,max}$. For $M_0 = 2.0$, for example, $M_c = 1.0$ when $\theta_c = 36.4^\circ$, whereas $\theta_{c,max} = 41^\circ$. The difference between critical and maximum cone angle is greater than the difference between critical and maximum plane-surface inclination (fig. 7) because there is an additional adiabatic compression between shock and cone surface. In fact, a small range of cone angles exists for each M_0 for which the flow behind the shock is partly supersonic and partly subsonic; the subsonic flow is nearest the cone surface.

The range of cone angles for which a mixed subsonic-supersonic field exists is determined by finding the limiting θ_c for $M_c = 1.0$ and for $M_1 = 1.0$. Using the curves for $M_0 = 2.0$, it is found from figure 7(a) that $M_1 = 1.0$ when the angle of deflection through the shock λ is 22.7°. For this value of λ, φ from figure 4 is 61.3°. From figure 8, the cone half-angle that produces this shock angle is determined to be 38.9°. This angle is then the limiting θ_c for which the entire field behind the shock is subsonic. The surface

velocity, however, was already sonic for $\theta_c = 36.4^\circ$ (fig. 11). From $\theta_c = 36.4^\circ$ to 38.9°, the subsonic-flow sector therefore increases gradually from the cone surface to the shock surface.

Determination of other flow variables. - In the appendix it is shown that the velocity at any point depends only on the Mach number at the point and upon the critical velocity, which is determined by free-stream conditions. The relation is plotted in dimensionless form in figure 12. From this figure, the velocity at the cone surface q_c may be determined when M_c has been found from figure 11. Similarly the velocity immediately behind the shock q_1, or on the surface of an inclined plane, may be determined when the Mach number M_1 has been found from figure 7. With the velocity ratio and Mach number ratio known, the ratio of sound velocities may easily be calculated. The density ratio is then obtained (because $a^2 = \gamma p/\rho$) from $\rho/\rho_0 = p/p_0 \, (a_0/a)^2$ and the static-temperature ratio, from $t/t_0 = (a/a_0)^2$.

Two-dimensional expansion around corners. - The charts presented have been concerned with flow conditions resulting from compressive deflection of the free stream. For the case of two-dimensional objects, there are also simple relations to determine conditions after an expansion through any given angle from given initial conditions. These relations result from the Prandtl-Meyer theory of supersonic flow around corners. The theory itself will not be given but may be found in reference 5. According to this theory, the Mach number and the static pressure are functions only of the angle through which the flow is turned.

These relations are plotted in figure 13, with the turning angle ν as abscissa and the corresponding Mach number M, ratio of static to total pressure p/P, and Mach angle β as ordinates. This chart is based on the initial condition that $M = 1.0$ for zero flow deflection ($\nu = 0$). The equations (19) and (20) used to plot these relations are given in the appendix. In order to use the chart for any other initial Mach number (within the range of the chart), it may be assumed that the flow has already been deflected through an angle ν_1, which corresponds to the initial Mach number M_1 assumed. The conditions of the flow following an expansion of λ degrees around a corner may then be obtained by reading the ordinates for an abscissa $\nu = \nu_1 + \lambda$. Because the Prandtl-Meyer theory is valid only for isentropic flow, it is only approximately accurate for compressive deflections resulting in shock waves. If the total-pressure loss through the shock is negligible, however, figure 13 may also be used to determine conditions resulting from compressive

deflection. For such compressive turning, conditions after a deflection of λ degrees are found by reading the ordinates at $\psi = \psi_1 - \lambda$, where ψ_1 is the abscissa corresponding to the initial conditions. The accuracy of the approximation may be checked by obtaining corresponding values from the shock charts (figs. 6 and 7). The use of the chart is illustrated in the following example: An airfoil with a symmetrical-diamond profile having edge angles of 20° is placed in a uniform air stream of Mach number $M_0 = 2.0$ at an angle of attack of 0. (See sketch, fig. 13.) The conditions in field (1) are determined from the shock charts. From figure 6(a), the static-pressure ratio across the shock emanating from the leading edge is found to be 1.70; the total-pressure ratio, from figures 4 and 3 is 0.983. The ratio of static pressure to total pressure behind the shock is therefore

$$p_1/P_1 = (1.70/0.983)(p_0/P_0)$$

where p_0/P_0 is a simple function of Mach number and may be obtained from figure 13. For $M_0 = 2.0$, $p_0/P_0 = 0.127$; hence, $p_1/P_1 = 0.220$. For this ratio, it is found from the same set of curves that $M_1 = 1.64$. These values are the initial conditions for the subsequent expansion through 20° around the midpoint of the profile. The abscissa on figure 13 for these conditions ($M_1 = 1.64$) is $\psi = 16.2^\circ$. The abscissa for the conditions after the expansion is $\psi = 16.2^\circ + 20^\circ = 36.2^\circ$. The conditions on the rear surfaces of the airfoil are now read for this abscissa: $M_2 = 2.38$, $p_2/P_1 = 0.072$.

The Mach angle β is useful if it is desired to plot the expansion region; the expansion takes place through a wedge-shaped region

bounded by lines making angles of $\beta_1 + 10^\circ = 37.2^\circ + 10^\circ = 47.2^\circ$ and $\beta_2 - 10^\circ = 24.8^\circ - 10^\circ = 14.8^\circ$, respectively, with the free-stream direction.

More complete charts for the determination of flow conditions following expansion around corners may be found in reference 10.

Flight Propulsion Research Laboratory,
National Advisory Committee for Aeronautics,
Cleveland, Ohio, January 15, 1947.

APPENDIX - EQUATIONS USED FOR COMPUTING CHARTS

A derivation of the equations that hold across an oblique shock may be found in reference 1. The relations given in that reference are modified somewhat and rewritten in terms of more convenient variables. The modifications made are as follows:

The relations between the static-pressure ratio across a shock p_1/p_0, the angle of deflection through the shock λ, and the shock angle φ, are as follows (reference 1, p. 238, equations 2.6 and 2.7, notations modified)

$$\sin^2 \varphi = \frac{\left[(\gamma - 1) + (\gamma + 1)\frac{p_1}{p_0}\right](\gamma - 1)}{4\gamma\left[\left(\frac{p_0}{p_0}\right)^{\frac{\gamma-1}{\gamma}} - 1\right]} \tag{1}$$

$$\frac{\tan(\varphi - \lambda)}{\tan(90 - \varphi)} = \frac{(\gamma - 1) + (\gamma + 1)\frac{p_1}{p_0}}{(\gamma + 1) + (\gamma - 1)\frac{p_1}{p_0}} = \frac{\rho_1}{\rho_0} \tag{2}$$

Because the quantity in the bracket of the denominator of equation (1) is equal to $\frac{\gamma - 1}{2} M_0^2$, equation (1) may be algebraically converted to

$$\frac{\frac{p_1}{p_0} - 1}{\gamma M_0^2} = (\sin^2 \varphi - 1/M_0^2)(1 - k^2) \tag{3}$$

where

$$k^2 = \frac{\gamma - 1}{\gamma + 1}$$

An alternative form of equation (2), which gives λ as an explicit function of φ or p_1/p_0, may be derived. In the notation of figure 1, the conservation of mass flow, momentum, and energy equations may be written

Mass:

$$\rho_0 N_0 = \rho_1 N_1 \tag{4}$$

Momentum:

$$L_0 = L_1 \tag{5a}$$

$$p_0 + \rho_0 N_0^2 = p_1 + \rho_1 N_1^2 = \text{constant} \tag{5b}$$

Energy:

$$\frac{a_0^2}{\gamma - 1} + \frac{q_0^2}{2} = \frac{a_1^2}{\gamma - 1} + \frac{q_1^2}{2} = \frac{a_{cr}^2}{2k^2} \tag{6}$$

From equation (6),

$$\frac{a_{cr}^2}{q_0^2} = k^2 + \frac{1 - k^2}{M_0^2} \tag{7}$$

From these equations, the velocity components in the horizontal and vertical directions are found to be (fig. 1):

$$u_1 = L_1 \cos \varphi + N_1 \sin \varphi$$

$$= q_0 \cos^2 \varphi + \frac{(a_{cr}^2 - k^2 q_0^2 \cos^2 \varphi) \sin \varphi}{q_0 \sin \varphi}$$

$$= (1 - k^2)\, q_0 \cos^2 \varphi + a_{cr}^2/q_0 \tag{8}$$

$$v_1 = L_1 \sin \varphi - N_1 \cos \varphi$$

$$= \cot \varphi \left\{ q_0 \left[1 - (1 - k^2) \cos^2 \varphi\right] - a_{cr}^2/q_0 \right\} \tag{9}$$

where N_1 was determined from the relation

$$N_0 N_1 = a_{cr}^2 - k^2 L^2$$

derived from equations 4 to 6.

The equation for λ is now found by dividing equation (9) by equation (8) and rearranging terms and symbols with the help of equations (3) and (7):

$$\tan \lambda = \frac{\left(\frac{\frac{p_1}{p_0} - 1}{\gamma M_0^2}\right) \cot \varphi}{1 - \left(\frac{\frac{p_1}{p_0} - 1}{\gamma M_0^2}\right)} \tag{10}$$

Equations (3) and (10) were used to plot figures 4 to 6. For $M_0 = \infty$, equation (3) becomes

$$\frac{\frac{p_1}{p_0} - 1}{\gamma M_0^2} = (1 - k^2) \sin^2 \varphi \tag{11}$$

and equation (10) becomes

$$\tan \lambda = \frac{(1 - k^2) \sin^2 \varphi \cot \varphi}{1 - (1 - k^2) \sin^2 \varphi} \tag{12}$$

The ratio M_1/M_0 plotted in figure 7 was obtained from the identity

$$\frac{M_1}{M_0} = \frac{q_1}{q_0} \left(\frac{p_0}{p_1} \frac{\rho_1}{\rho_0}\right)^{1/2} \tag{13}$$

The ratio q_1/q_0 may be determined from equation (8):

$$\frac{q_1}{q_0} \cos \lambda = \frac{u_1}{q_0} = \frac{(1 - k^2) q_0 \cos^2 \varphi + \frac{a_{cr}^2}{q_0}}{q_0}$$

which may be written as

$$\frac{q_1}{q_0} \cos \lambda = \cos^2 \varphi + \frac{a_{cr}^2}{q_0^2} - k^2 \cos^2 \varphi$$

$$= 1 - \left(\sin^2 \varphi - \frac{a_{cr}^2}{q_0^2} + k^2 \cos^2 \varphi\right)$$

$$= 1 - \frac{\frac{p_1}{p_0} - 1}{\gamma M_0^2} \tag{14}$$

The quantity ρ_1/ρ_0 is obtained from equation (2)

$$\frac{\rho_1}{\rho_0} = \frac{\frac{P_1}{P_0} + k^2}{k^2 \frac{P_1}{P_0} + 1} \tag{15}$$

Figures 3 and 12, which apply for all flow across compression shocks, may be determined from the above relations. For the ratio of total pressure across the shock, the general compressible-flow relation may be used:

$$\frac{P_1}{P_0} = \frac{p_1}{p_0}\left[\frac{1 + \frac{\gamma-1}{2} M_1^2}{1 + \frac{\gamma-1}{2} M_0^2}\right]^{\frac{\gamma}{\gamma-1}} \tag{16}$$

Because P_1/P_0 and M_1 are both functions only of λ and M_0 (figs. 5 to 7) and, because λ is a function only of M_0 and φ (fig. 4), the ratio P_1/P_0 may be plotted as a function of φ for various M_0, as shown in figure 3.

Equation (7) shows that the free-stream velocity depends only on the critical velocity and the free-stream Mach number. Because a_{cr} is constant across a shock, equation (7) holds for all velocities before and after the shock. The ratio of any velocity to the free-stream velocity may therefore be written in the following form:

$$\left(\frac{q}{q_0}\right)^2 = \left(\frac{a_{cr}^2 M^2}{k^2 M^2 + 1 - k^2}\right)\left(\frac{k^2 M_0^2 + 1 - k^2}{a_{cr}^2 M_0^2}\right)$$

$$= \left(\frac{M}{M_0}\right)\frac{\frac{\gamma-1}{2} M_0^2 + 1}{\frac{\gamma-1}{2} M^2 + 1} = \frac{1 + \frac{\gamma-1}{2} M_0^2}{\left(\frac{M_0}{M}\right) + \frac{\gamma-1}{2} M_0^2} \tag{17}$$

Equation (17) is plotted in figure 12 and may be used to determine the velocity immediately after a shock q_1 if M_1 has been determined or to determine the velocity at the cone surface q_c if M_c has been found.

The Mach number at the cone surface is determined from isentropic compression relations if the pressure and Mach number immediately after the shock and the pressure at the cone surface are known. The relation is

$$M_c^2 = \frac{2}{\gamma-1}\left[\frac{1 + \frac{\gamma-1}{2} M_1^2}{\left(\frac{p_c}{p_1}\right)^{\frac{\gamma-1}{\gamma}}} - 1\right] \tag{18}$$

where p_1, M_1, and p_c may be determined from figures 6, 7, and 10, respectively. The ratio M_c/M_0 is plotted against θ_c in figure 11. The angle of deflection through the shock λ, from which p_1 and M_1 are determined, is found from figure 4 when the shock angle φ has been determined from figure 8.

The derivation of the Prandtl-Meyer relations for flow around corners is given in reference 5. In the notation of this paper and with the initial condition that $\psi = 0$ when $M = 1.0$, these relations (plotted in fig. 13) are given by the following equations:

$$\psi = \frac{1}{k}\tan^{-1}\left(k\sqrt{M^2 - 1}\right) + \sin^{-1}\frac{1}{M} - 90^\circ$$

$$= \frac{1}{k}\tan^{-1}(k \cot \beta) + \beta - 90^\circ \tag{19}$$

$$\frac{p}{P} = \left(1 + \frac{\gamma-1}{2} M^2\right)^{-\frac{\gamma}{\gamma-1}}$$

$$= \left[(1 - k^2)\cos^2 k(\psi - \beta + 90^\circ)\right]^{\frac{\gamma}{\gamma-1}} \tag{20}$$

REFERENCES

1. Taylor, G. I., and Maccoll, J. W.: Oblique Shock Waves. Vol. III of Aerodynamic Theory, div. H, ch. IV, sec. 2, W. F. Durand, ed., Julius Springer (Berlin), 1935, pp. 236-241. (Reprinted, C.I.T., Jan. 1943.)

2. Taylor, G. I., and Maccoll, J. W.: The Air Pressure on a Cone Moving at High Speeds. - I and II. Proc. Roy. Soc. (London), ser. A, vol. 139, no. 838, Feb. 1, 1933, pp. 278-311.

3. Maccoll, J. W.: The Conical Shock Wave Formed by a Cone Moving at a High Speed. Proc. Roy. Soc. (London), ser. A, vol. 159, no. 898, April 1, 1937, pp. 459-472.

4. Hantzsche, W., and Wendt, H.: Mit Überschallgeschwindigkeit angeblasene Kegelspitzen. Tech. Bericht, ZWB, Bd. 9, Nr. 7, Dez. 1942, pp. 24-34.

5. Taylor, G. I., and Maccoll, J. W.: The Two-Dimensional Flow Around a Corner; Two-Dimensional Flow Past a Curved Surface. Vol. III of Aerodynamic Theory, div. H, ch. IV, sec. 5-6, W. F. Durand, Ed., Julius Springer (Berlin), 1935, pp. 243-249. (Reprinted, C.I.T., Jan. 1943.)

6. Busemann, A.: Conical Supersonic Flow with Axial Symmetry. British R.T.P. Trans. No. 1598, Ministry Aircraft Prod. (From Luftfahrtforschung, vol. 19, no. 4, June 5, 1942, pp. 137-144.)

7. Ferrari, C.: Determination of the Pressure Exerted on Solid Bodies of Revolution with Pointed Noses Placed Obliquely in a Stream of Compressible Fluid at Supersonic Velocity. British R.T.P. Trans. No. 1105, Ministry Aircraft Prod. (From Atti della Reale Accad. delle Sci. di Torino, vol. 72, Nov.-Dec. 1936, pp. 140-163.)

8. Busemann, Adolf: Infinitesimale keglige Überschallströmung. Sonderdruck aus dem Jahrb. 1942/43, d. D. Akad. d. Luftfahrtforschung, Dez. 4, 1942. (Infinitesimal Concial Supersonic Flow. Trans. CGD-114, Douglas Aircraft Co., Inc.)

9. Ferri, A.: Experiments at Supersonic Speed on a Biplane of the Busemann Type. British R.T.P. Trans. No. 1407, Ministry Aircraft Prod. (From Atti Guidonia No. 37-38, Oct. 11, 1940, pp. 517-557.)

10. Ivey, Reese H., Stickle, George W., and Schuettler, Alberta: Charts for Determining the Characteristics of Sharp-Nose Airfoils in Two-Diminsional Flow at Supersonic Speeds. NACA TN No. 1143, 1947.

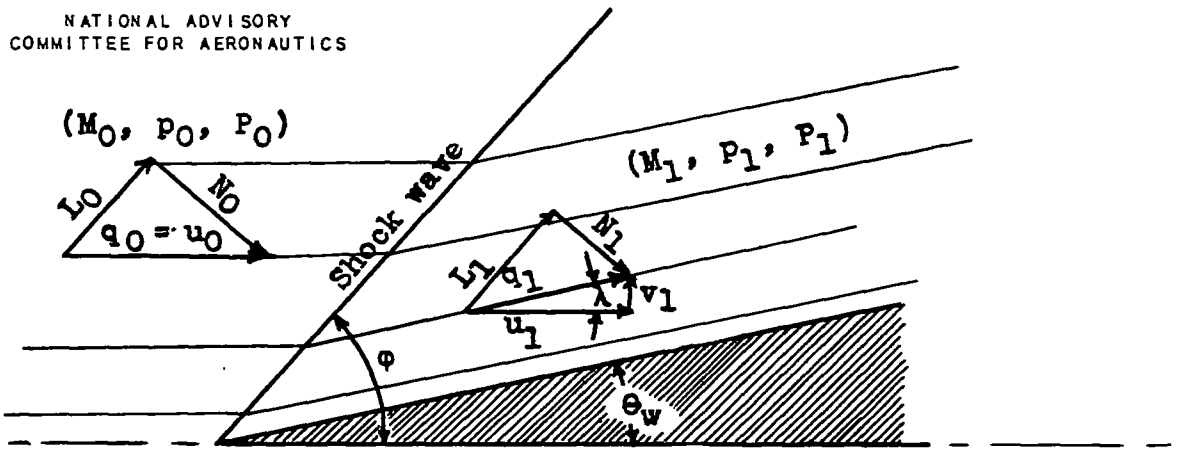

Figure 1.- Supersonic flow over inclined plane surface of infinite span and chord.

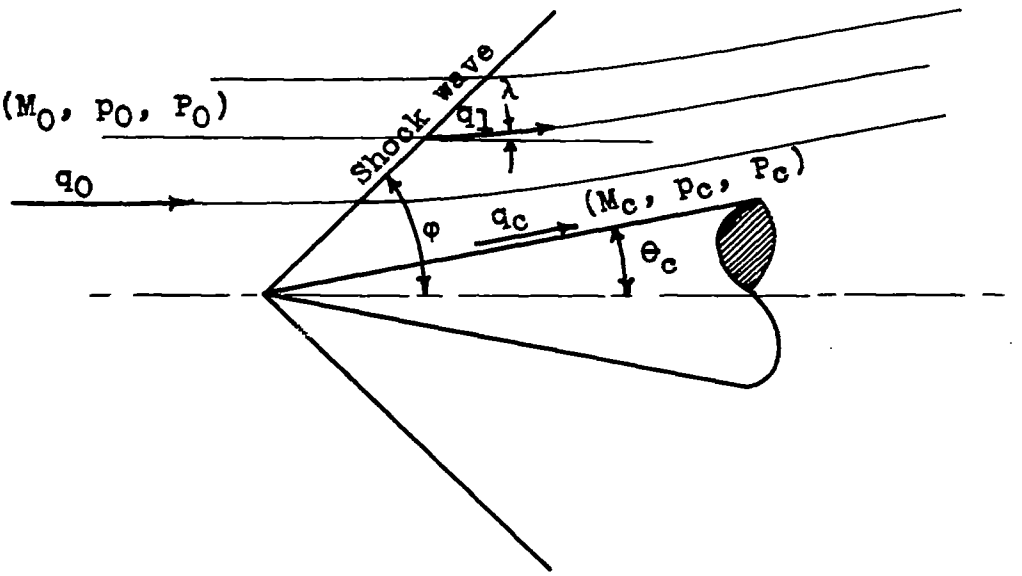

Figure 2.- Supersonic flow over axially symmetric cone.

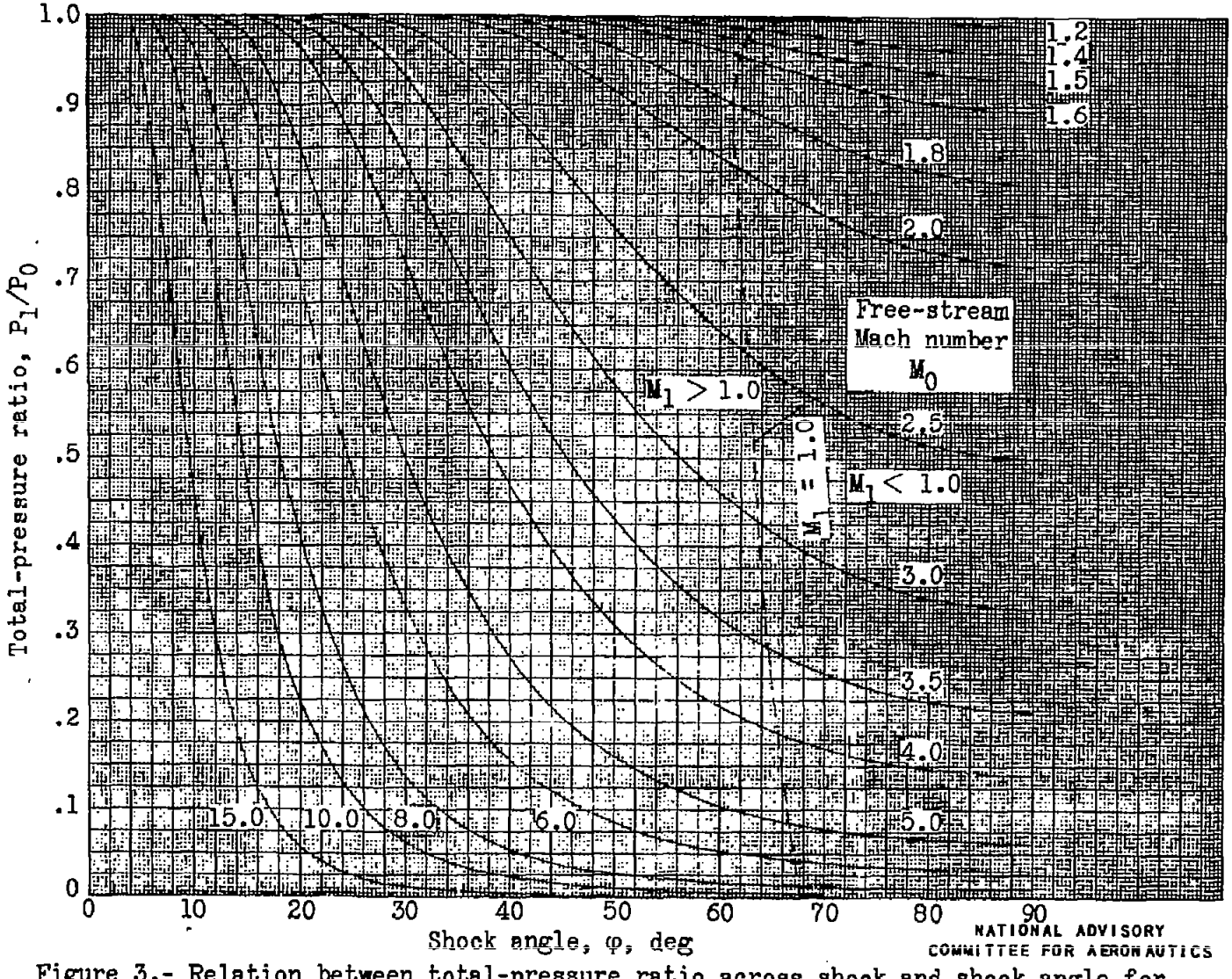

Figure 3.- Relation between total-pressure ratio across shock and shock angle for various free-stream Mach numbers. γ, 1.40.

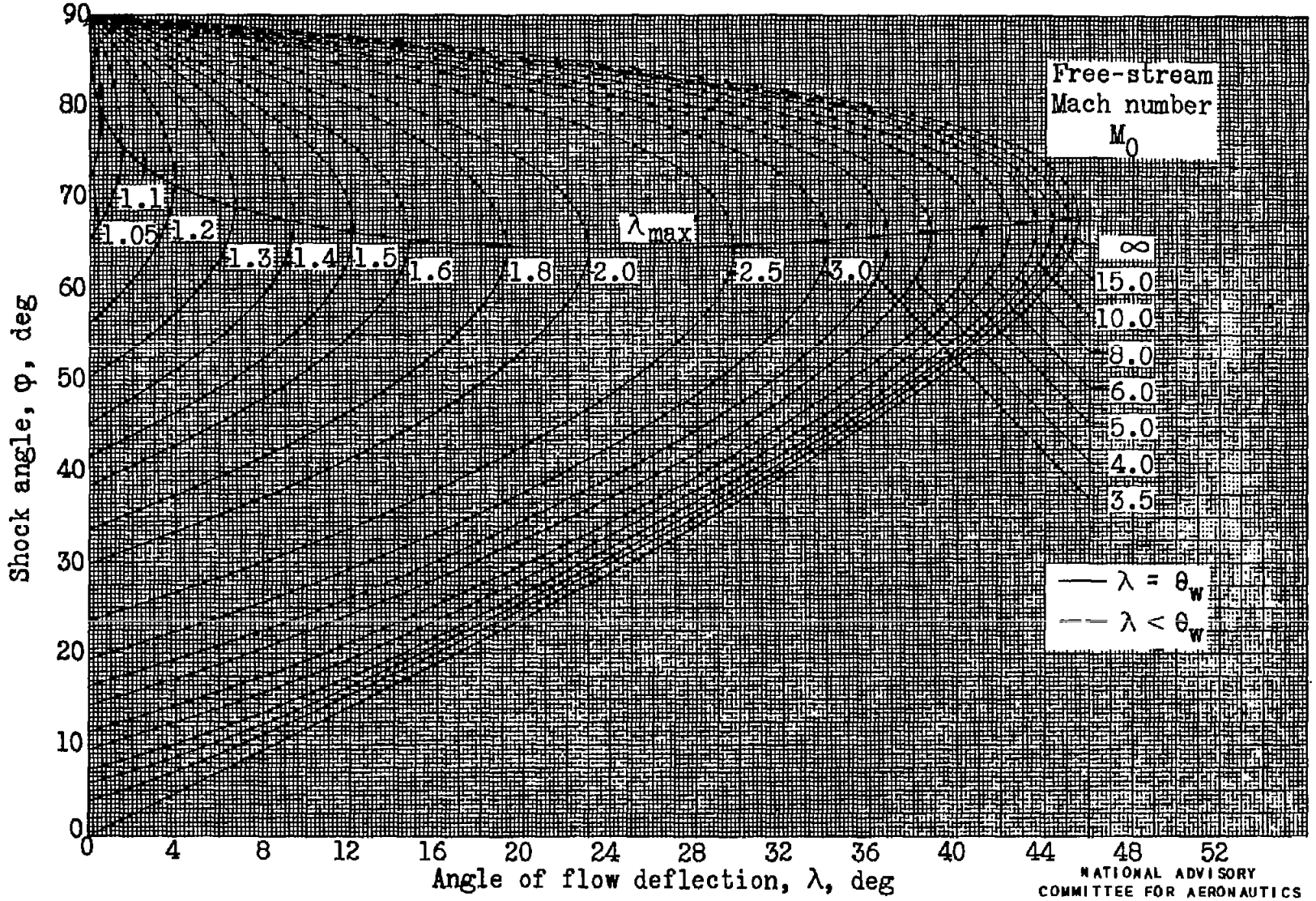

Figure 4.- Relation between shock angle and angle of flow deflection for various free-stream Mach numbers. γ, 1.40.

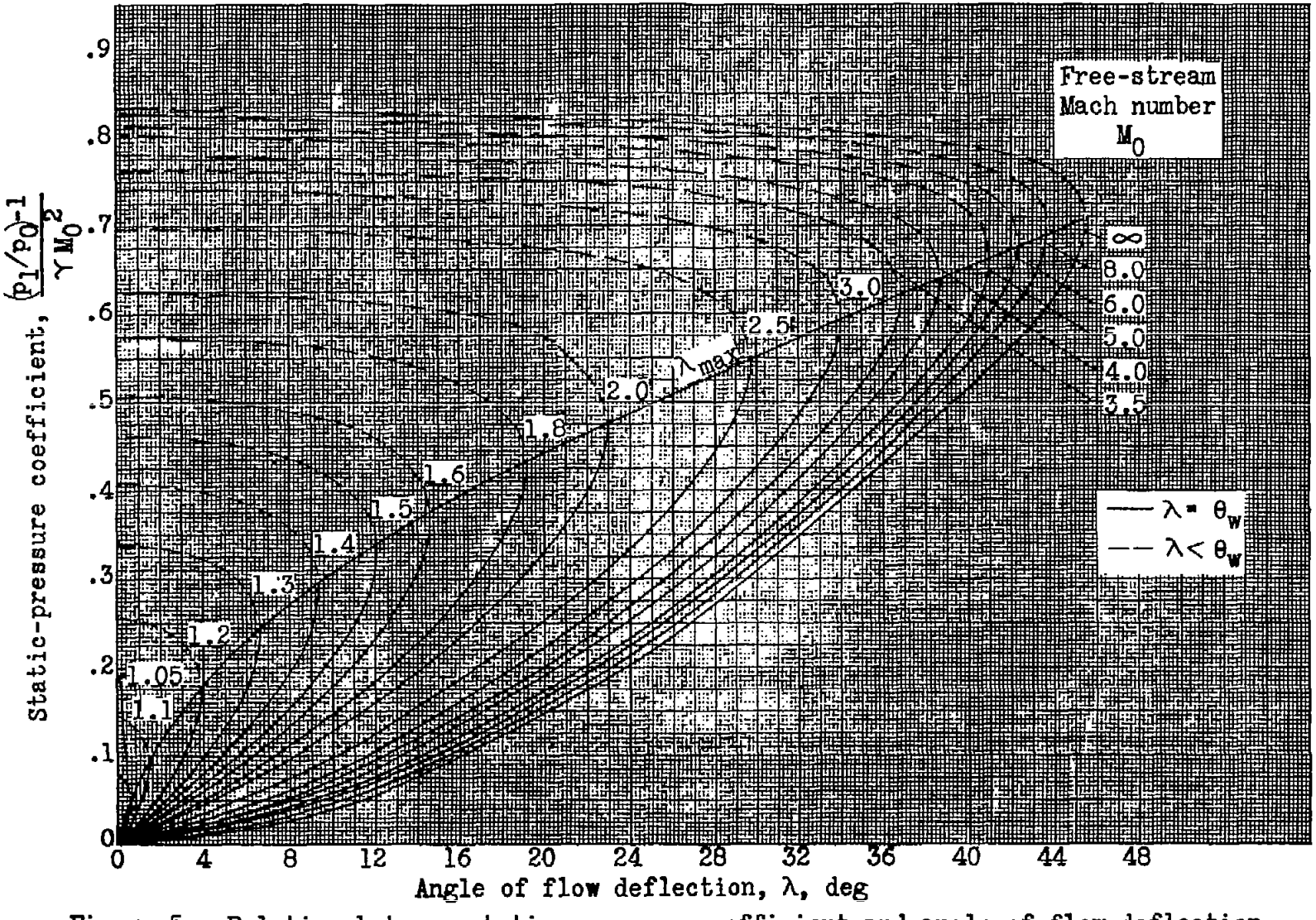

Figure 5.- Relation between static-pressure coefficient and angle of flow deflection for various free-stream Mach numbers. γ, 1.40.

NATIONAL ADVISORY COMMITTEE FOR AERONAUTICS

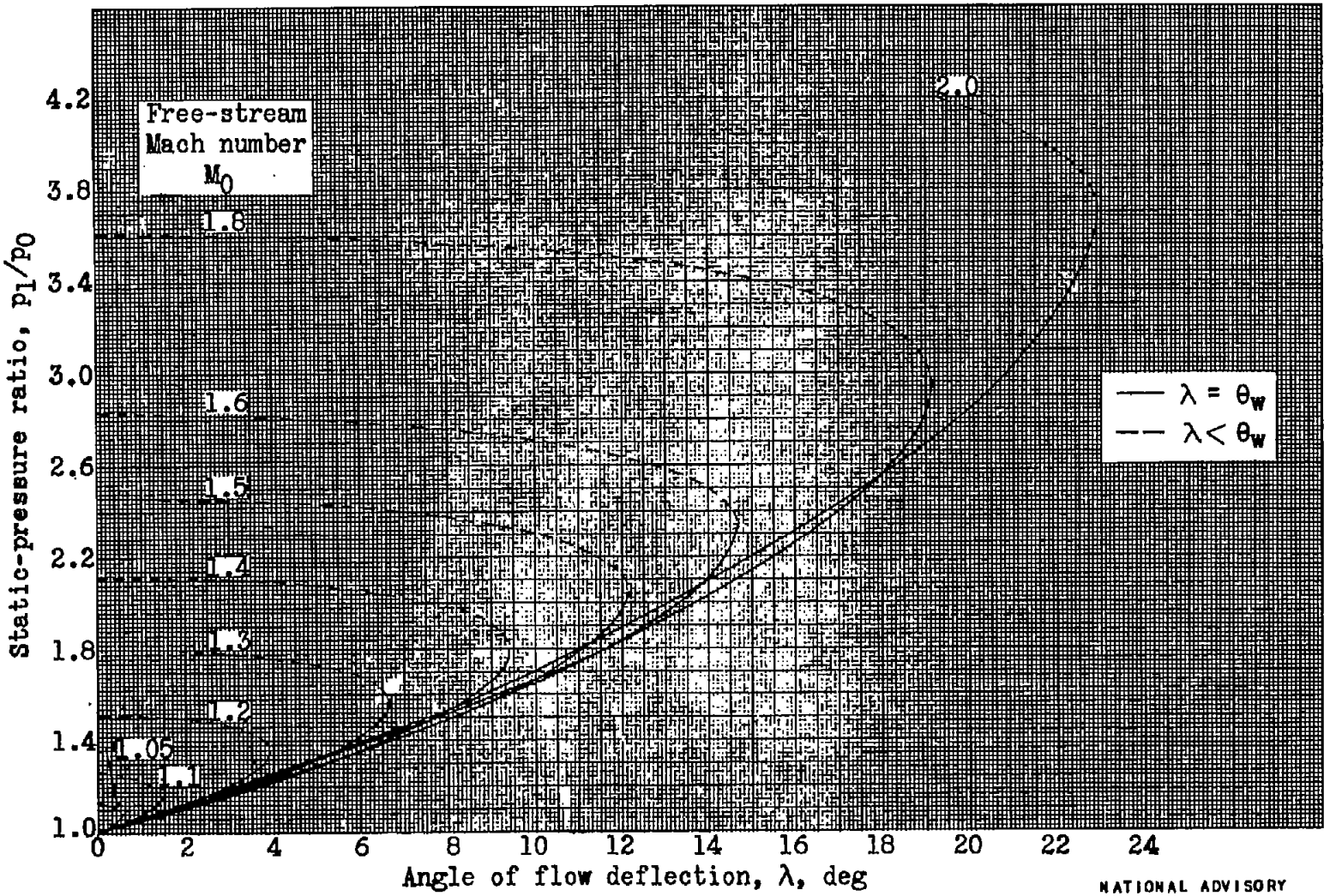

(a) M_0, 1.05 to 2.0.

Figure 6.- Relation between static-pressure ratio across shock and angle of flow deflection for various free-stream Mach numbers. γ, 1.40.

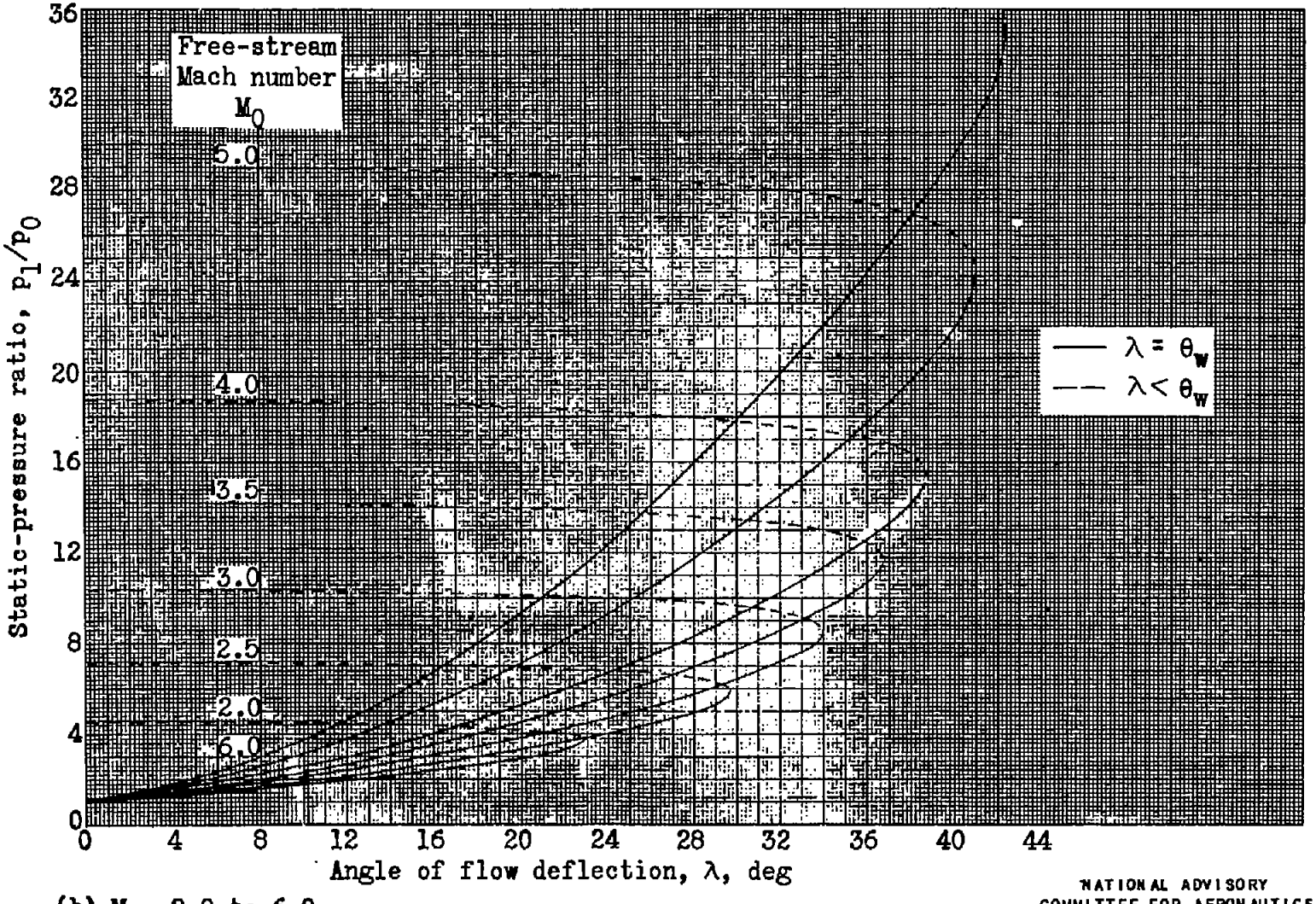

NATIONAL ADVISORY
COMMITTEE FOR AERONAUTICS

(b) M_0, 2.0 to 6.0.

Figure 6.- Continued. Relation between static-pressure ratio across shock and angle of flow deflection for various free-stream Mach numbers. γ, 1.40.

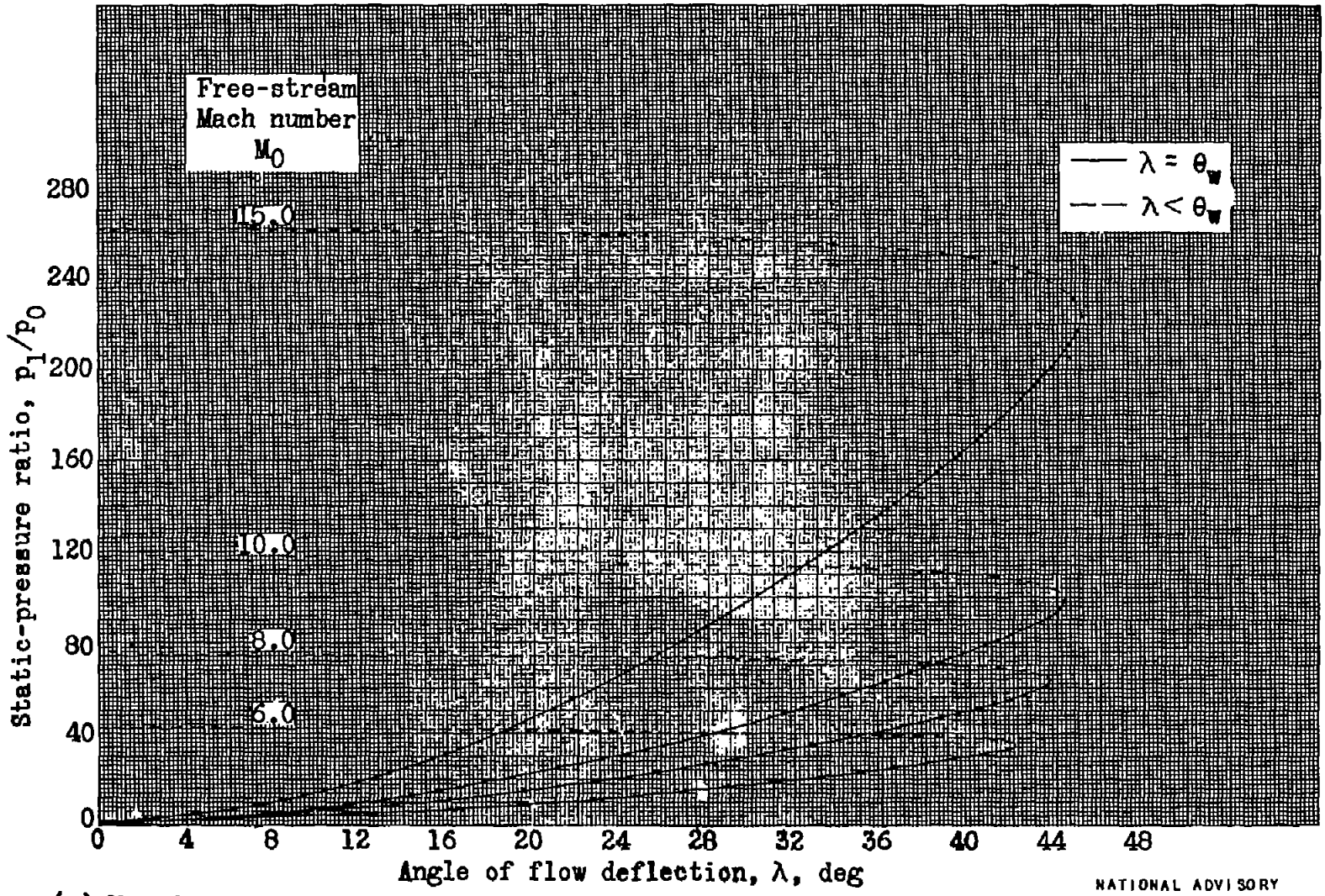

(c) M_0, 6.0 to 15.0.

Figure 6.- Concluded. Relation between static-pressure ratio across shock and angle of flow deflection for various free-stream Mach numbers. γ, 1.40.

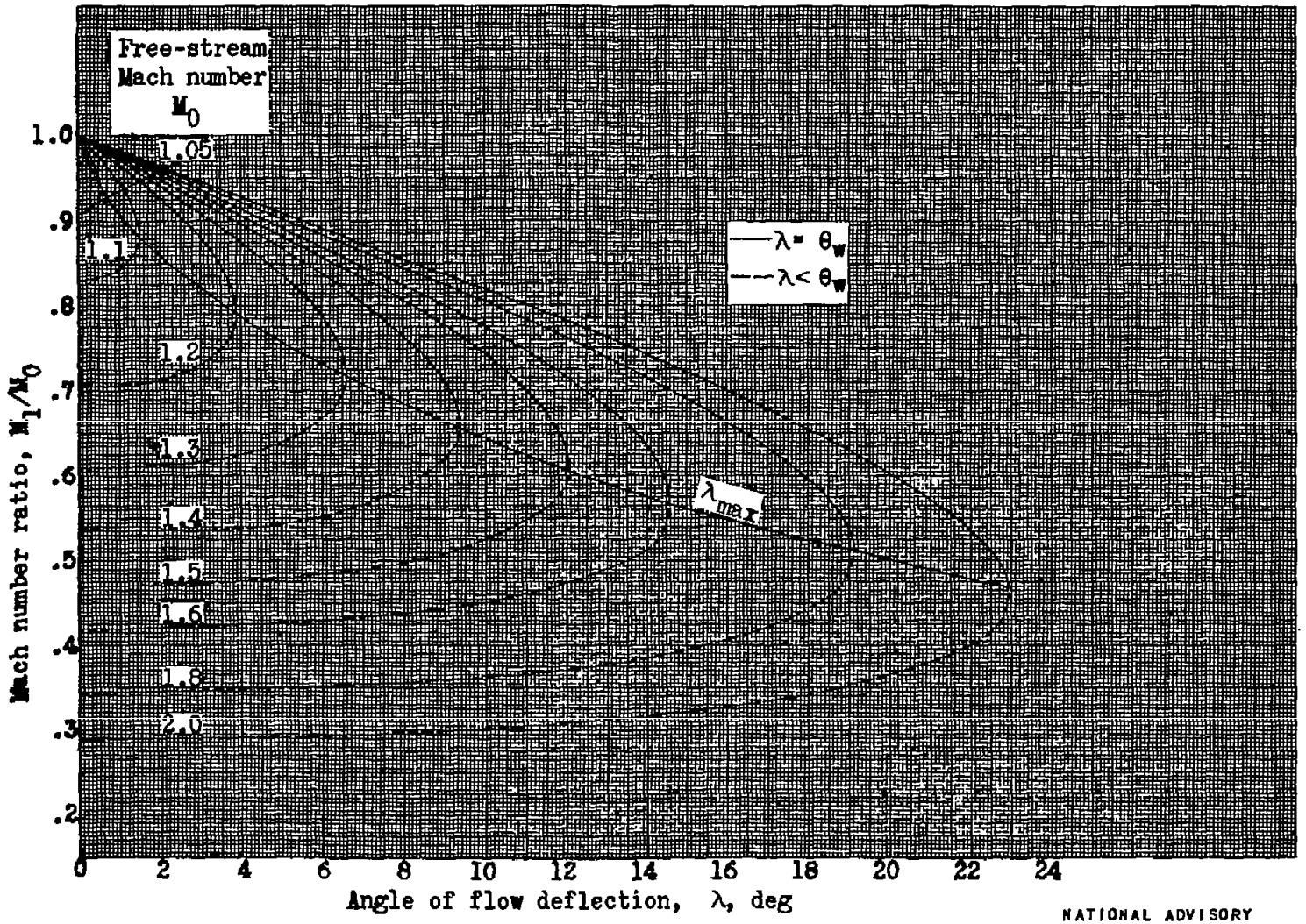

NATIONAL ADVISORY COMMITTEE FOR AERONAUTICS

(a) M_0, 1.05 to 2.0.

Figure 7.- Relation between Mach number ratio across shock and angle of flow deflection for various free-stream Mach numbers. γ, 1.40.

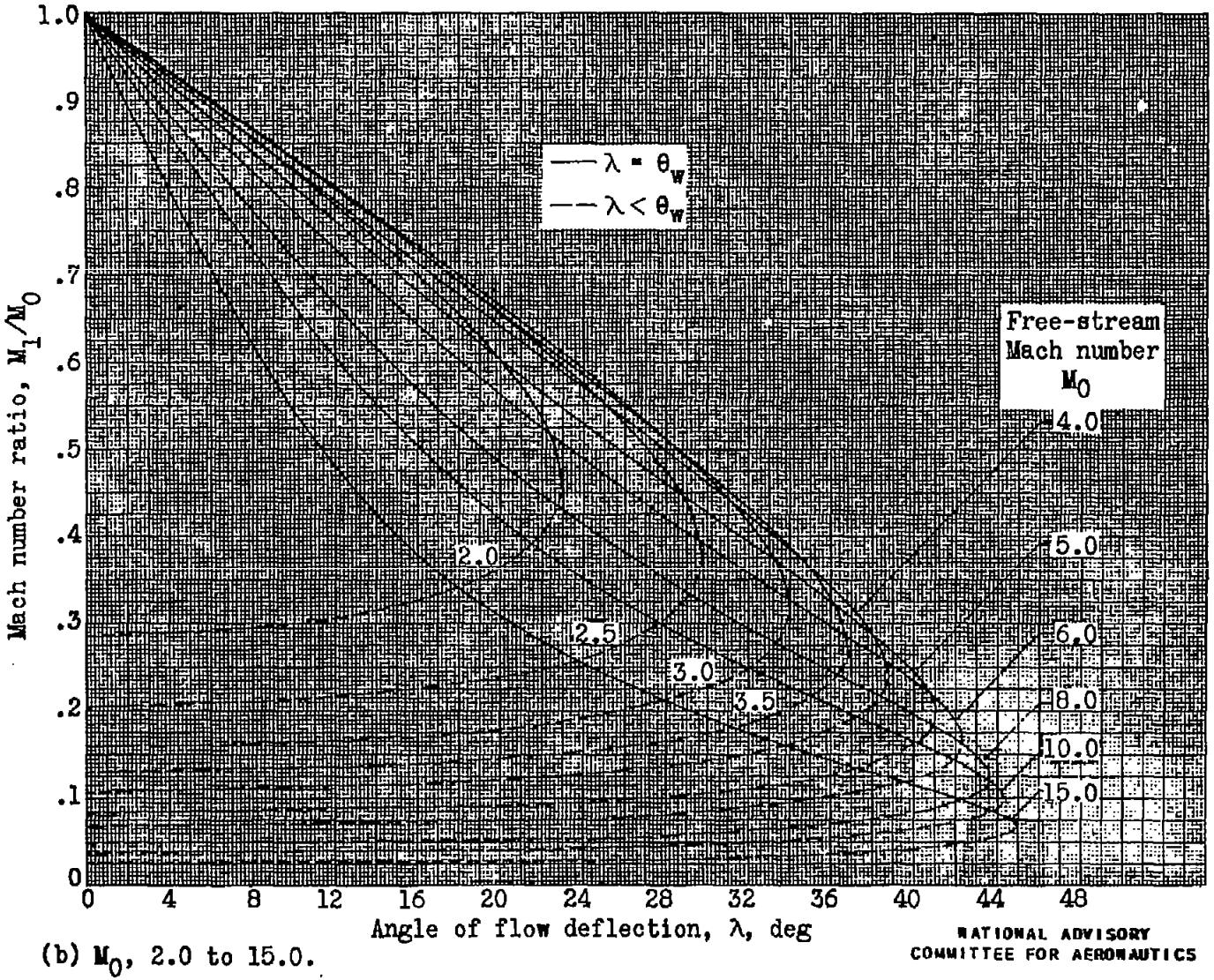

(b) M_0, 2.0 to 15.0.

Figure 7.- Concluded. Relation between Mach number ratio across shock and angle of flow deflection for various free-stream Mach numbers. γ, 1.40.

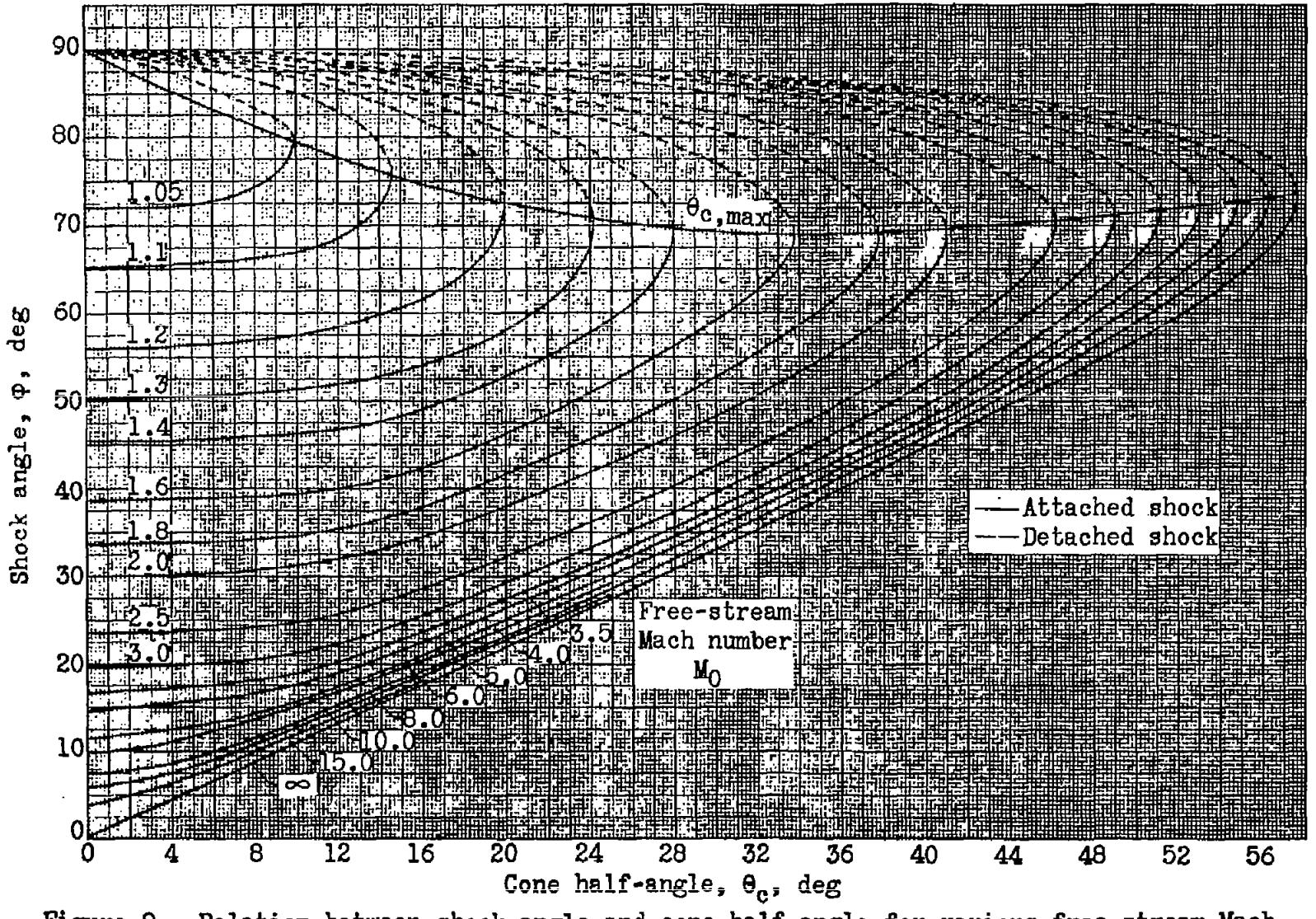

Figure 8.- Relation between shock angle and cone half-angle for various free-stream Mach numbers. γ, 1.40.

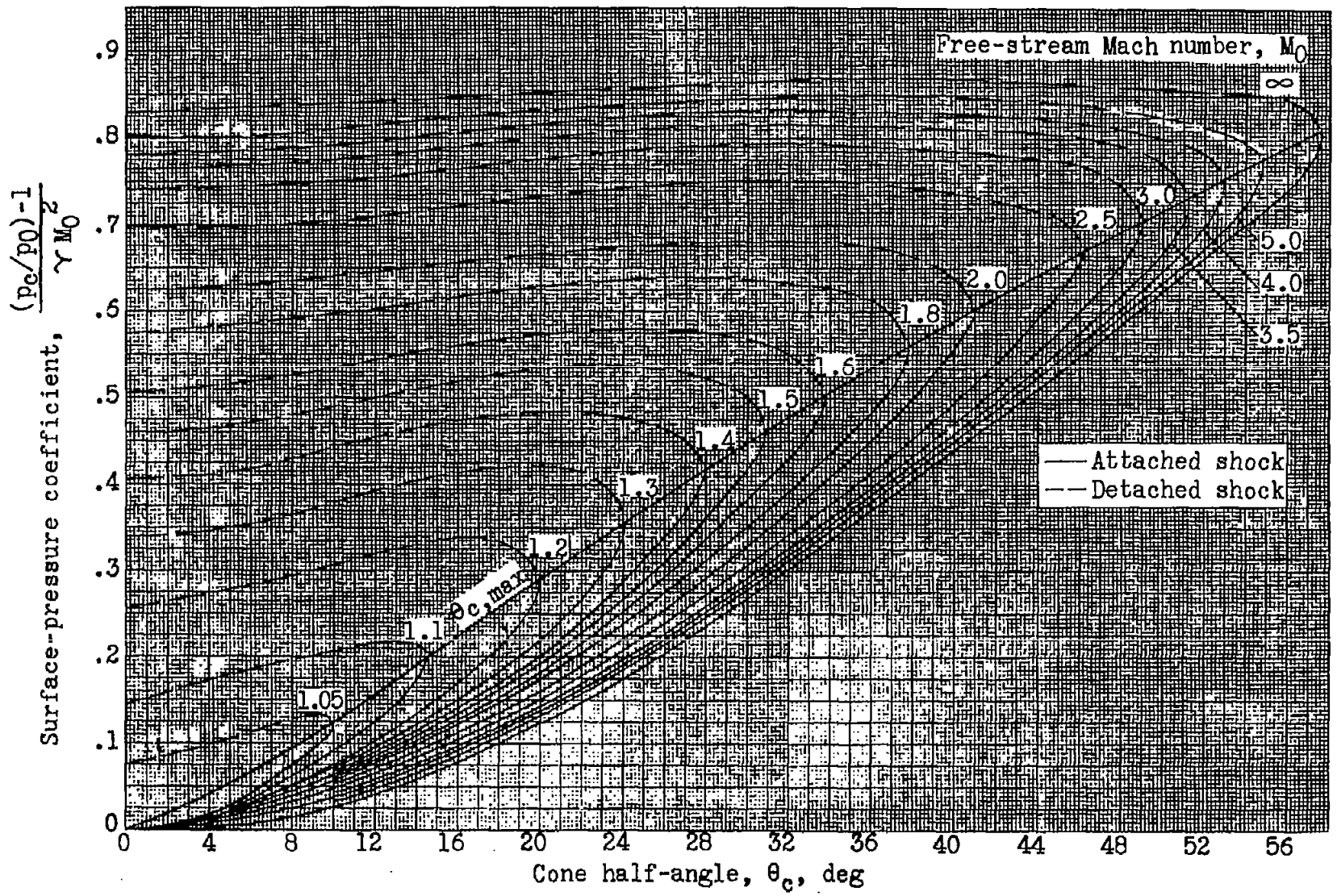

Figure 9.- Relation between surface-pressure coefficient and cone half-angle for various free-stream Mach numbers. γ, 1.40.

NATIONAL ADVISORY COMMITTEE FOR AERONAUTICS

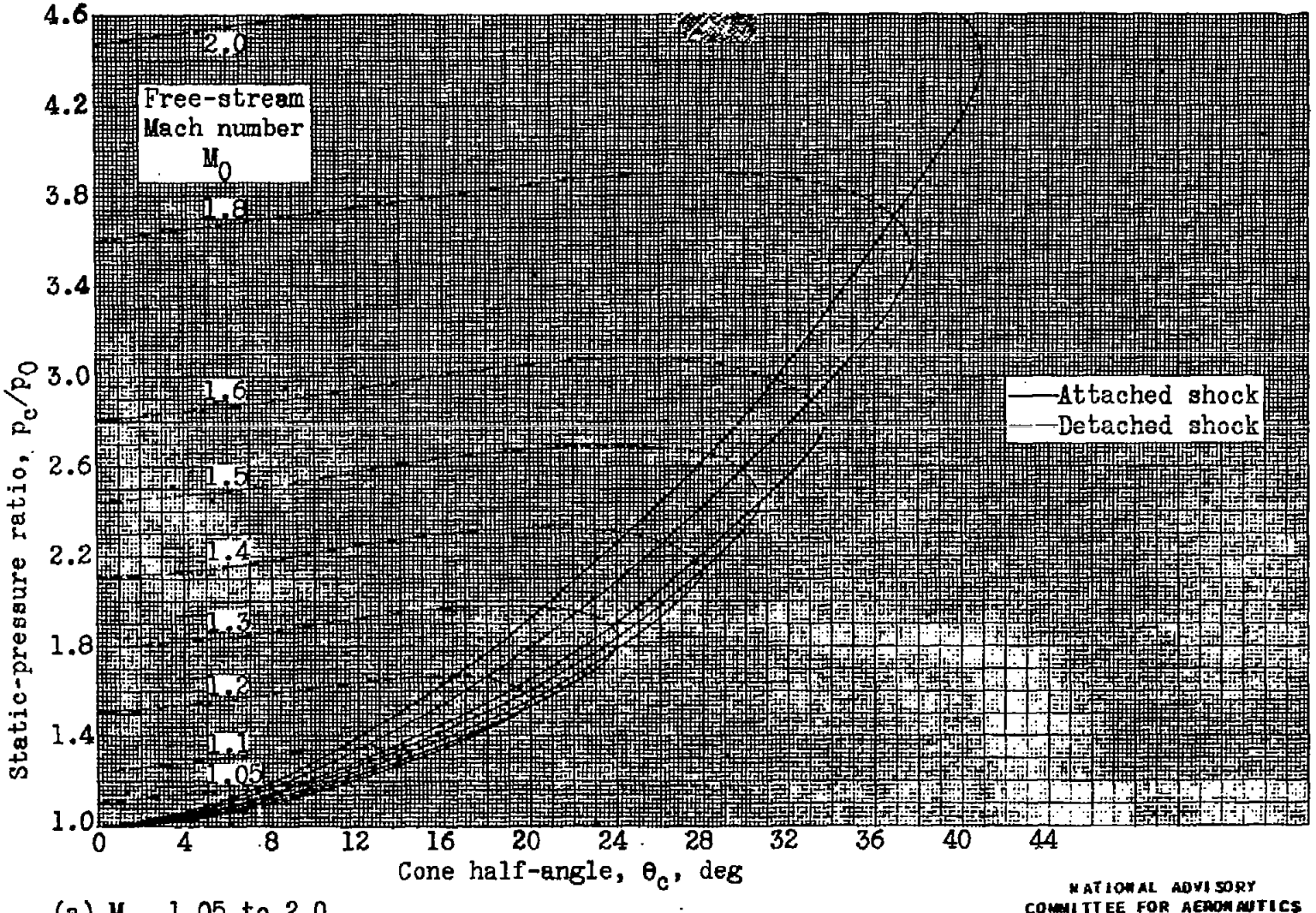

(a) M_0, 1.05 to 2.0.

Figure 10.- Relation between surface static-pressure ratio and cone half-angle for various free-stream Mach numbers. γ, 1.40.

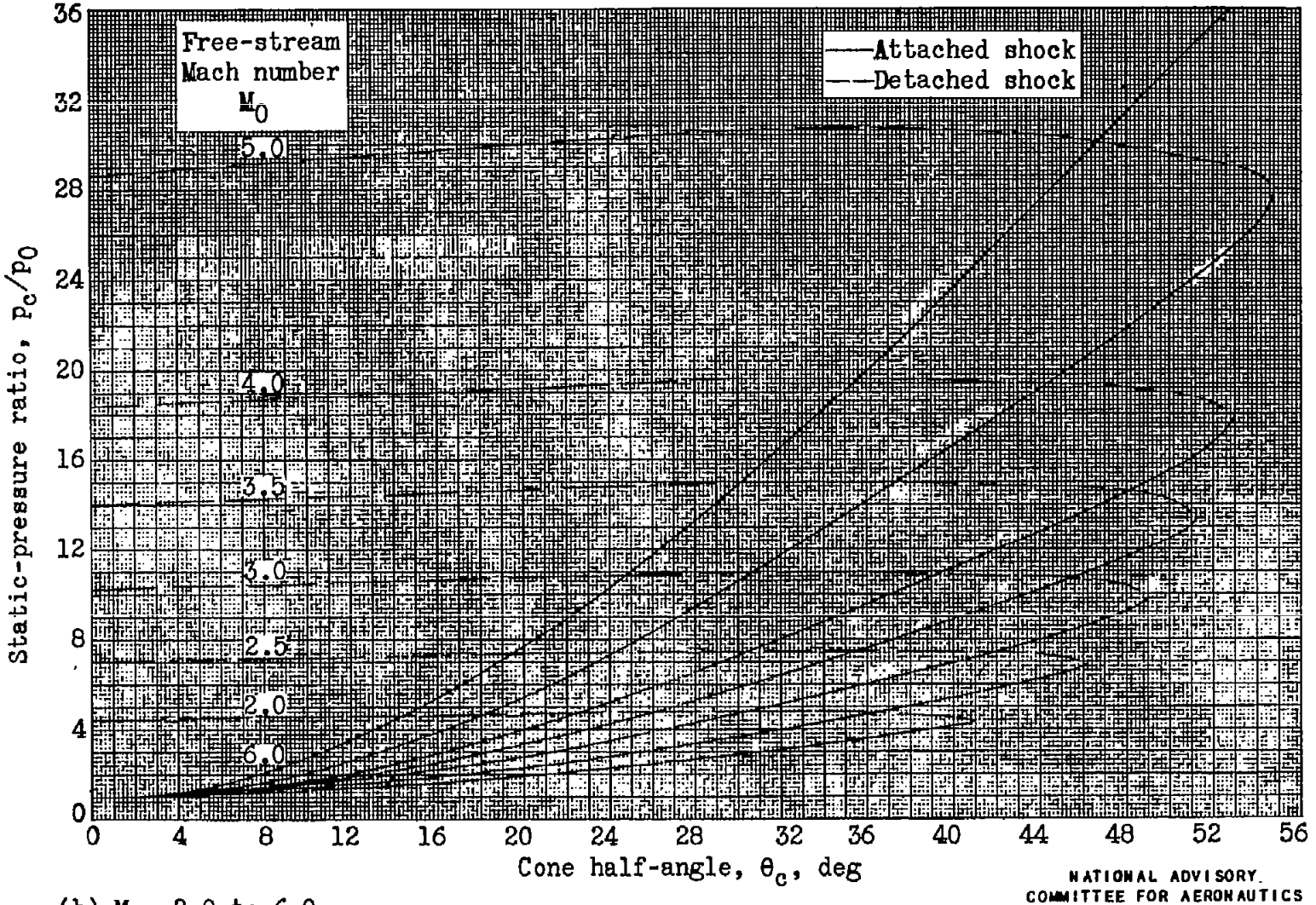

(b) M_0, 2.0 to 6.0.

Figure 10.- Continued. Relation between surface static-pressure ratio and cone half-angle for various free-stream Mach numbers. γ, 1.40.

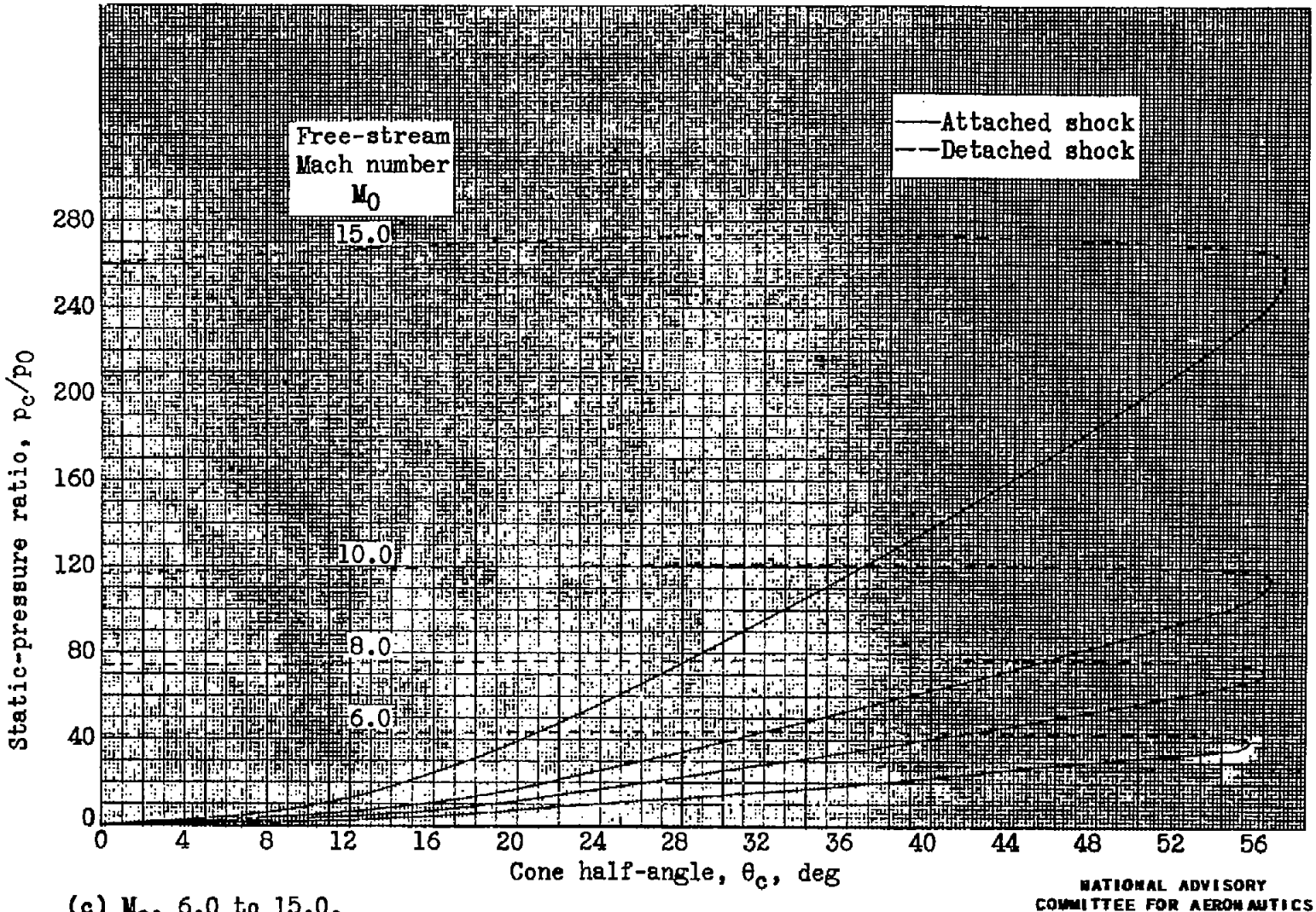

(c) M_0, 6.0 to 15.0.

Figure 10.- Concluded. Relation between surface static-pressure ratio and cone half-angle for various free-stream Mach numbers. γ, 1.40.

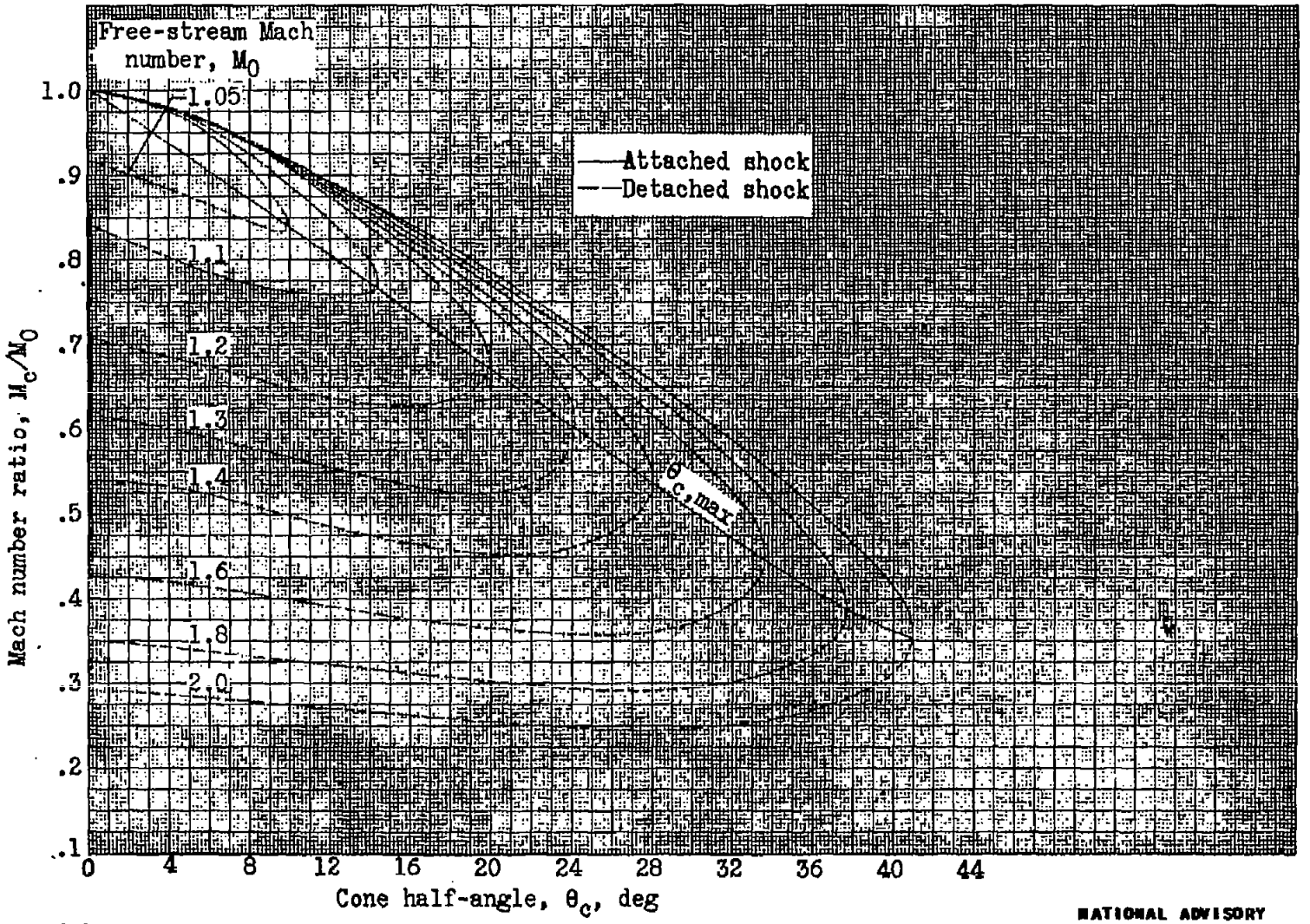

(a) M_0, 1.05 to 2.0.

NATIONAL ADVISORY COMMITTEE FOR AERONAUTICS

Figure 11.- Relation between surface Mach number ratio and cone half-angle for various free-stream Mach numbers. γ, 1.40.

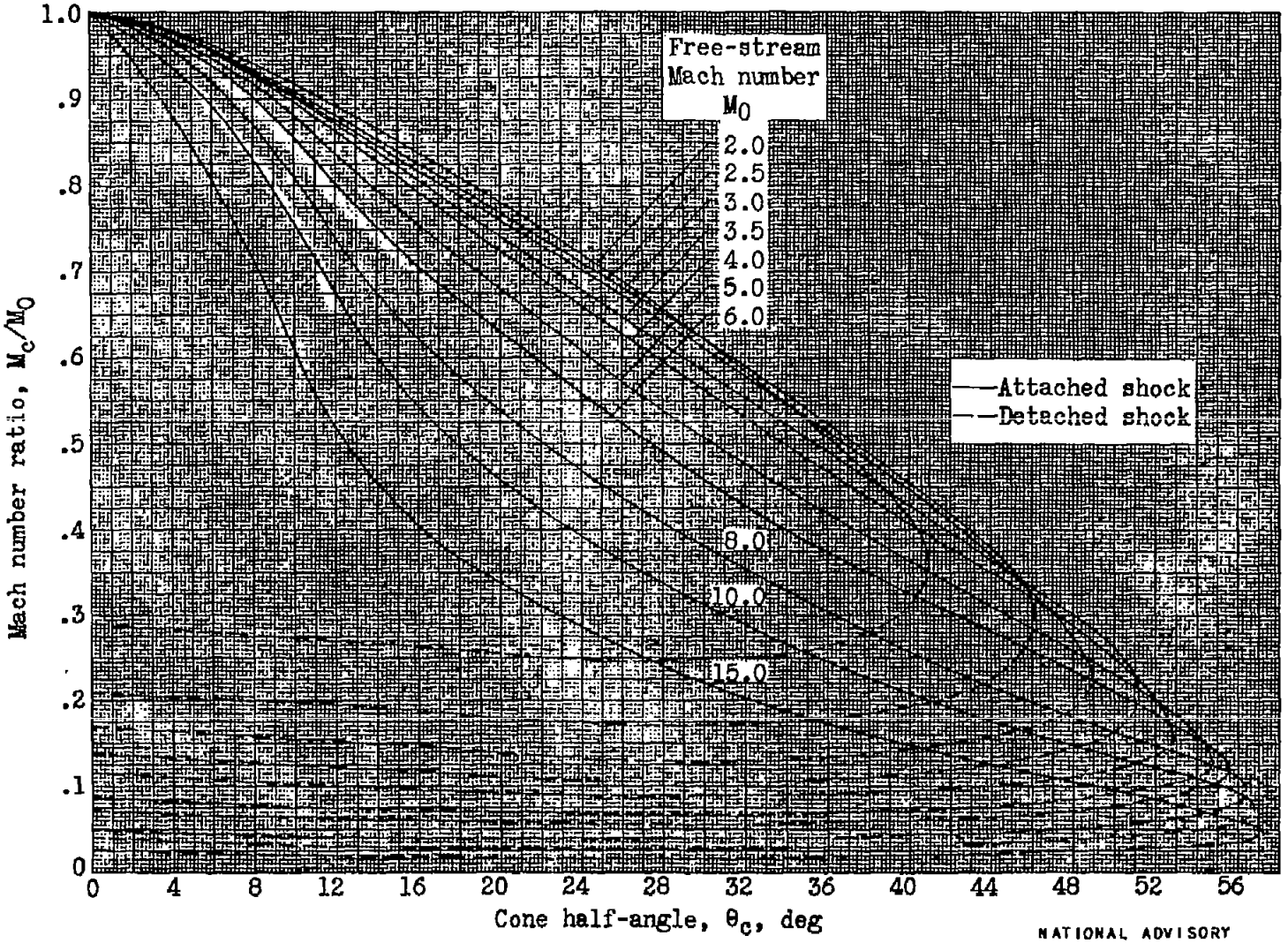

(b) M_0, 2.0 to 15.0.

Figure 11.- Concluded. Relation between surface Mach number ratio and cone half-angle for various free-stream Mach numbers. γ, 1.40.

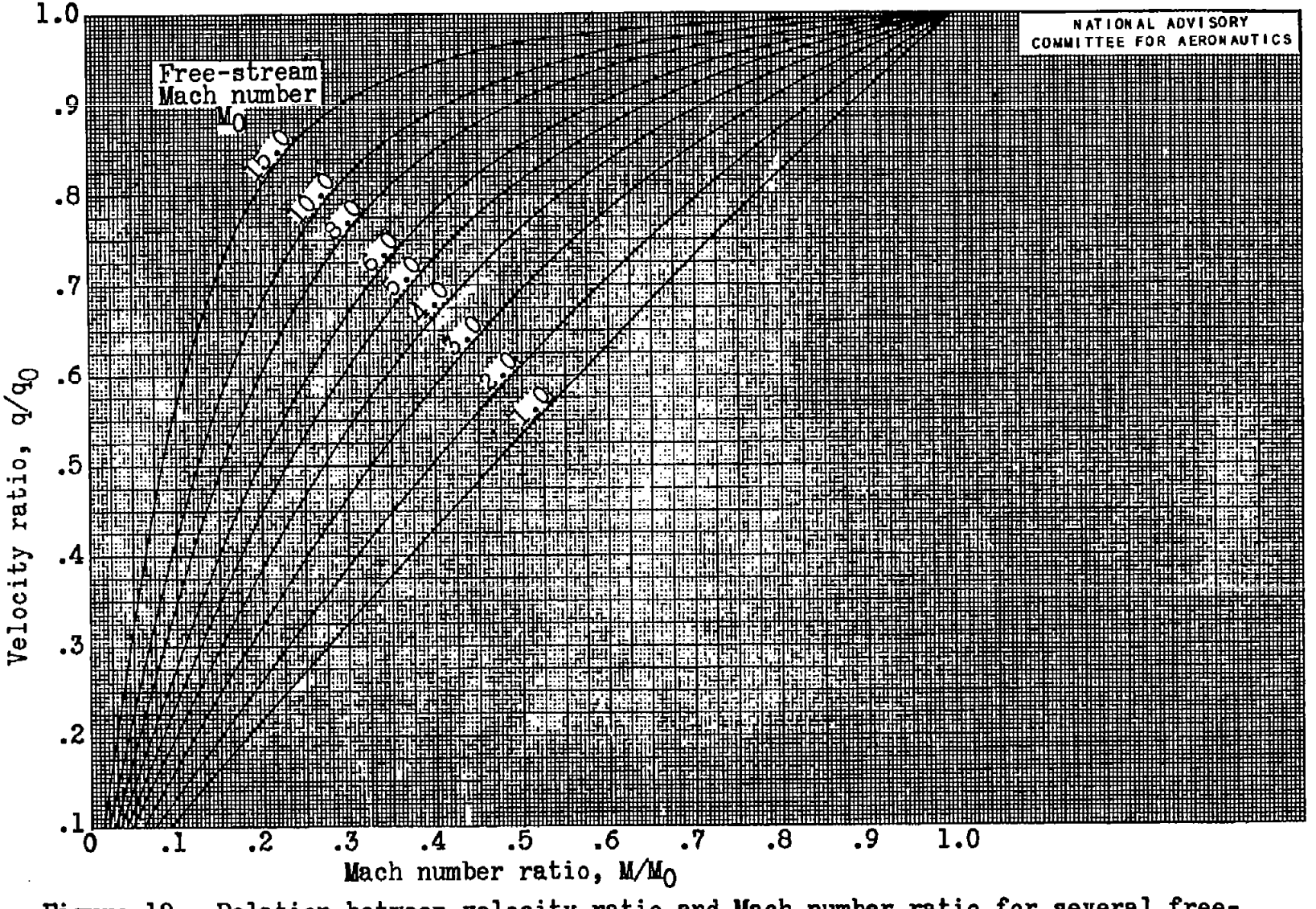

Figure 12.- Relation between velocity ratio and Mach number ratio for several free-stream Mach numbers. γ, 1.40.

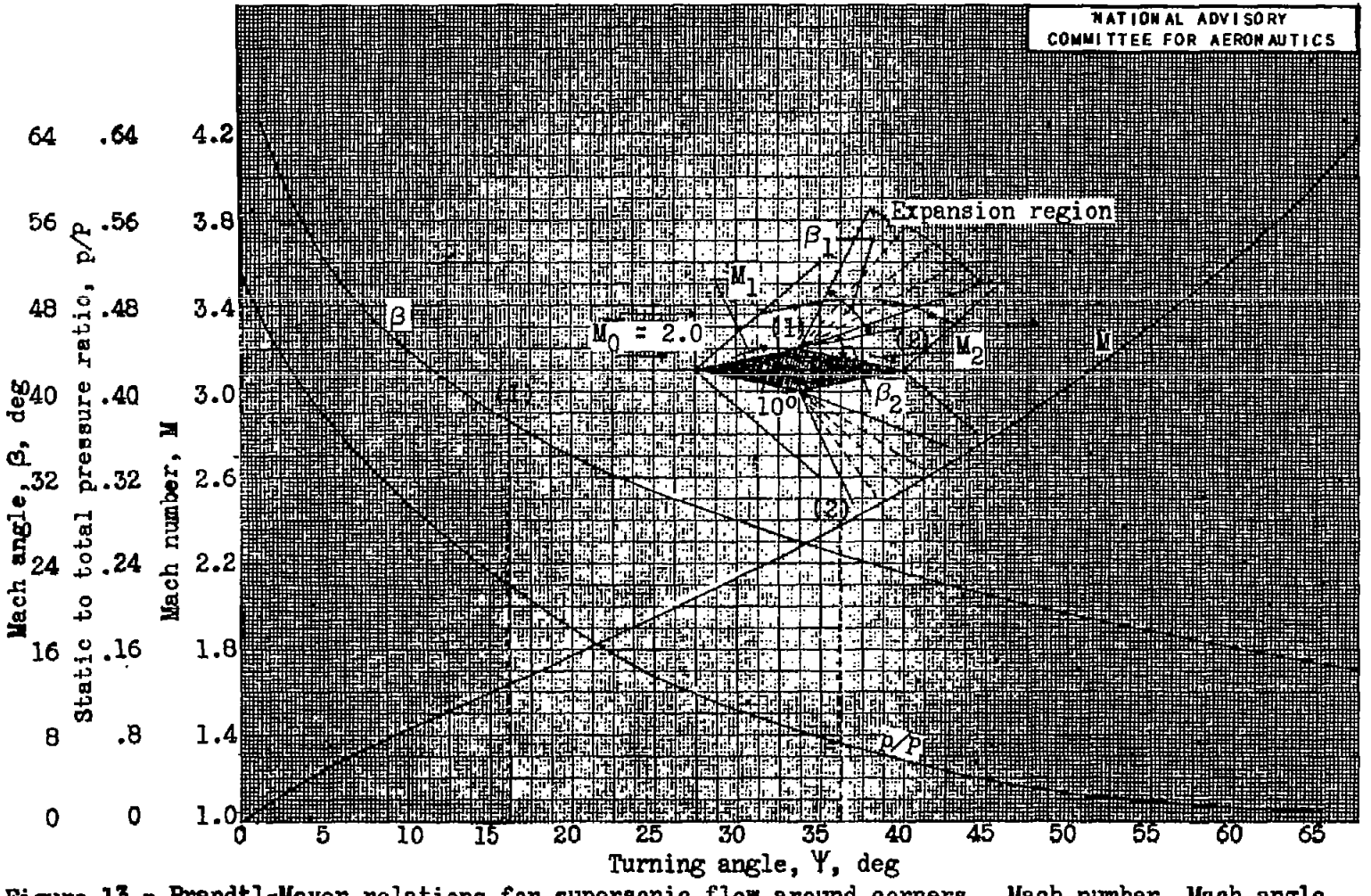

Figure 13.- Prandtl-Meyer relations for supersonic flow around corners. Mach number, Mach angle, and ratio of static to total pressure as functions of turning angle.

NACA - Langley Field, Va.